

Supplement for **Timing of exotic, far-travelled boulder emplacement and paleo-outburst flooding in the central Himalaya**

Marius L. Huber<sup>1,2</sup>, Maarten Lupker<sup>1</sup>, Sean F. Gallen<sup>3</sup>, Marcus Christl<sup>4</sup>, Ananta P. Gajurel<sup>5</sup>

---

**Supplement 1 (S1): Field survey and boulder provenance**

S1.1 Overview maps of field sites

**Samples on tributary fan, south of Devighat, “Trishuli downstream”**

Sampled boulders: NEQ/162 44, ...45, ...46 and ...47 and rocksample from “delta” boulder  
Many boulders spread on a tributary fan at the Trishuli River, south of Devighat



Figure S1.1-1: Google Earth, n. d., [satellite imagery for central Nepal], Retrieved June to November 2017, Google Earth Version 7.3.0

**Samples at fill terrace, Betrawati, “Trishuli upstream”**

Sampled boulders: NEQ/162 **60**, ...**61**, ...**66** and ...**67**.



Figure S1.1-2: Google Earth, n. d., [satellite imagery for central Nepal], Retrieved June to November 2017, Google Earth © 2016 DigitalGlobe

**Samples north of Betrawati “Trishuli upstream”**  
Sampled boulders: NEQ/162 **58**, and ...**59**.



Figure S1.1-3: Google Earth, n. d., [satellite imagery for central Nepal], Retrieved June to November 2017, Google Earth © 2016 DigitalGlobe

### Samples around Balephi, Sunkoshi/ Balephi Khola

Sampled boulders: NEQ/161 01, ...02 and ...03. And NEQ/162 79, ...80 and ...98.



Figure S1.1-4: Google Earth, n. d., [satellite imagery for central Nepal], Retrieved January 2020, Google Earth © 2020 CNES/Airbus

### S1.2 Sampled boulders in detail

- **NEQ/162 44** (“Trishuli downstream”)



*Figure S1.2-1*



*Figure S1.2-2*

**Orthogneiss** of Higher Himalayan origin.

- NEQ/162 45 (“Trishuli downstream”)



Figure S1.2-3



Figure S1.2-4



Figure S1.2-5

**Orthogneiss** of Higher Himalayan origin.

- NEQ/162 46 (“Trishuli downstream”)



Figure S1.2-6



Figure S1.2-7

**Orthogneiss** of Higher Himalayan origin.

- NEQ/162 47 (“Trishuli downstream”)



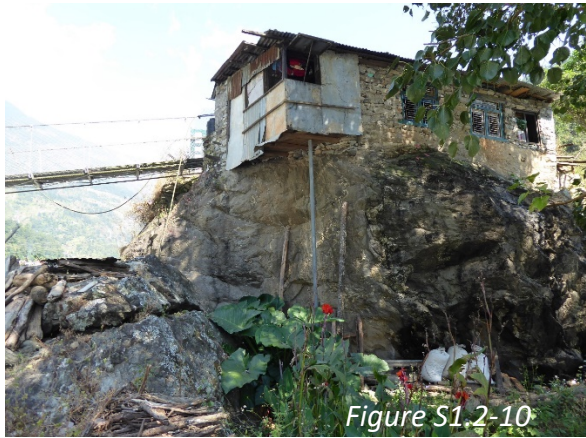
Figure S1.2-8



Figure S1.2-9

**Phyllitic schist** of Lesser Himalayan sequence, most likely Kuncha Formation within Nawakot Complex, Dandagaon Formation could also be possible.

- NEQ/162 58 (“Trishuli upstream”)



**Phyllite** of Lesser Himalayan sequence, most likely Kuncha Formation within Nawakot Complex, Dandagaon Formation could also be possible.

- NEQ/162 59 (“Trishuli upstream”)



Figure S1.2-15



Figure S1.2-16



Figure S1.2-17



Figure S1.2-18

Orthogneiss of Higher Himalayan origin.

- NEQ/162 60 (“Trishuli upstream”)



Figure S1.2-19



Figure S1.2-20

**Schist** of Lesser Himalayan sequence, most likely Kuncha Formation within Nawakot Complex  
Dandagaon Formation could also be possible.

- NEQ/162 61 (“Trishuli upstream”)



Figure S1.2-21



Figure S1.2-22

**Schist** of Lesser Himalayan sequence, most likely Kuncha Formation within Nawakot Complex, Dandagaon Formation could also be possible.

- NEQ/162 66 (“Trishuli upstream”)



Figure S1.2-23



Figure S1.2-24



Figure S1.2-25

**Schist** of Lesser Himalayan sequence, most likely Kuncha Formation within Nawakot Complex, Dandagaon Formation could also be possible.

- NEQ/162 67 (“Trishuli upstream”)

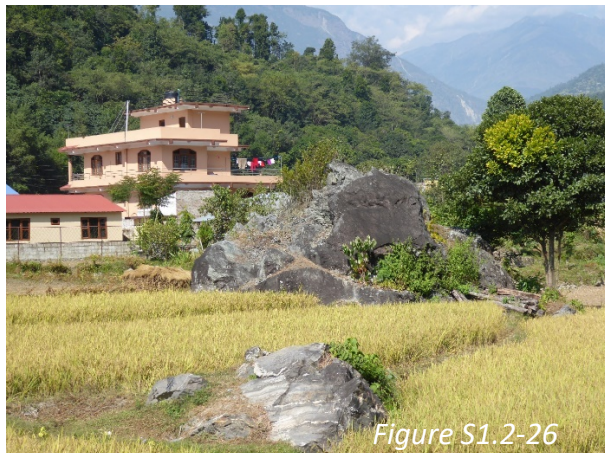


Figure S1.2-26



Figure S1.2-27



Figure S1.2-28

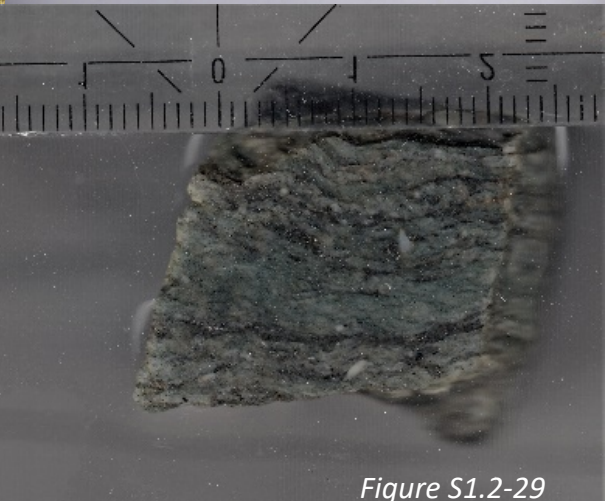


Figure S1.2-29

**Phyllitic schist** of Lesser Himalayan sequence, most likely Kuncha Formation within Nawakot Complex, Dandagaon Formation could also be possible. Different fabric than 47, 58, 60, 61 and 66.

- NEQ-161 01 (Sunkoshi)



Figure S1.2-30



Figure S1.2-31

**Orthogneiss** of Higher Himalayan Crystallines (no Lesser Himalayan sequence), with garnets, maybe with leucosomes, migmatitic, too homogenous for a paragneiss.

- NEQ/161 02 (Sunkoshi)



Figure S1.2-32

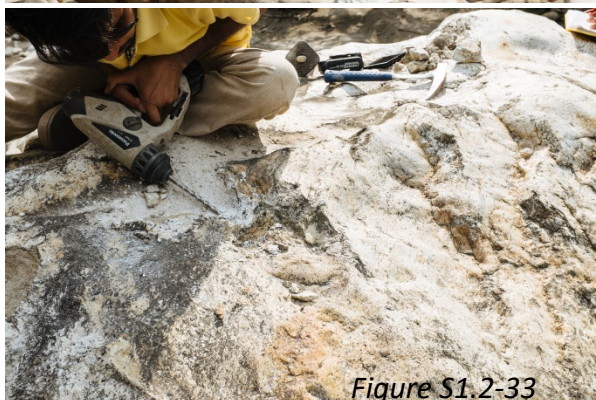


Figure S1.2-33



Figure S1.2-34

**whitish orthogneiss** of undifferentiated Higher Himalayan Crystallines (no lesser Himalayan sequence), no garnet found.

- NEQ/161 03 (Sunkoshi)



Figure S1.2-35



Figure S1.2-36



Figure S1.2-37

**Augengneiss, Ulleri-gneiss** of Higher Himalayan Crystallines (no Lesser Himalayan sequence), with garnets.

- NEQ/162 79 (Sunkoshi, Balephi Khola)



Figure S1.2-38



Figure S1.2-39

**Augengneiss**, possibly metagranitoide, of Higher Himalayan Crystallines (no Lesser Himalayan sequence)

- NEQ/162 80 (Sunkoshi)



Figure S1.2-40



Figure S1.2-41



Figure S1.2-42

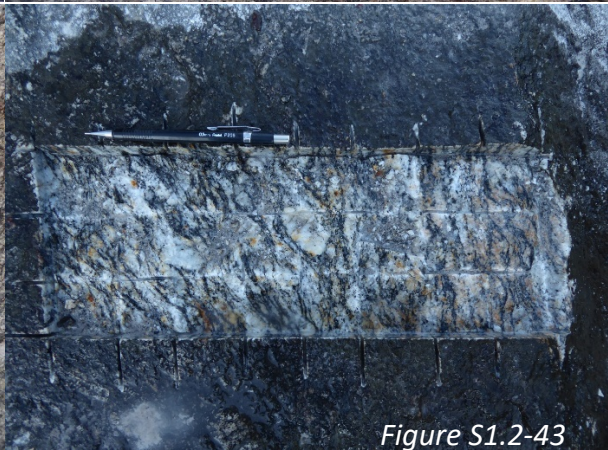


Figure S1.2-43

**Augengneiss** of Higher Himalayan Crystallines (no Lesser Himalayan sequence), structure quite common in the Higher Himalayan Crystallines.

- NEQ/162 98 (Sunkoshi, Balephi Khola)



Figure S1.2-44



Figure S1.2-45

**Augengneiss** of Higher Himalayan Crystallines (no Lesser Himalayan sequence), structure quite common in the Higher Himalayan Crystallines.

### S1.3 Fill-terraces at Betrawati and further downstream



Figure S1.3-A:  
Coordinates of viewpoint:  
27.96925, 85.18104  
Betrawati fill-terrace at river-cut seen from different angle than Figure 2B.  
Deposit has sorting, some grading and clast-supported texture. Surveyed boulder NEQ/162 66 with intermediate diameter of 8.8 m sitting on top. Photo credit K. Cook, GFZ Potsdam - 2017).



Figure S1.3-B:  
Coordinates of viewpoint:  
27.95223, 85.16403  
Large boulder (probably >10 m maximum diameter) spotted half-buried in fill-deposit approx. 3 km south of Betrawati terrace and “Trishuli upstream” boulders.  
Excavation of boulder after deposition by river incision likely (river behind utility pole).



Figure S1.3-C:  
Coordinates of viewpoint:  
27.94721, 85.16353  
Boulder of B seen from other angle (in red circle). Hydropower facility in the foreground.

## **Supplement 2 (S2): Paleo-hydrologic discharge estimation**

### *Topographic maps used for river channel cross-section extraction*

Topo-maps by the Government of Nepal, Survey Department produced in co-operation with the Government of Finland and the Finnish Meteorological Institute.

Following map sheets are covering the study area and were utilised for channel cross-section extraction (including scale and year of publication):

**2785 01B Nuwakot**, 1 : 25 000, 1996  
**2785 01C Devighat**, 1 : 25 000, 1996  
**2785 04 Barhabise**, 1 : 50 000, 1996  
**2785 08 Dadapakhar**, 1 : 50 000, 1996  
**2885 13 Somdan**, 1 : 50 000, 1997

*Cross-section site selecting was done with guidelines by Costa (1983), p.997.*

*Profiles were drawn with Matlab-function “manningseq” in supplementary material from Rosenwinkel et al. (2017), by Schwanghart.*

*Parameters, imported data and results generated with “bouldersforpaleohydrology” code-package (Matlab) accessible via URL <https://gitlab.com/mlh300/bouldersforpaleohydrology/>*

### **Basic parameters used for code [allochthonous\\_boulders\\_for\\_paleohydrology.m](#)**

Flood water density: **rho\_f = 1500 kg/m<sup>3</sup>**  
Gravitational acceleration: **g = 9.81 m/s<sup>2</sup>**

### **Basic parameters used for function [manningseq.m](#)**

Manning's roughness coefficient for mountain streams (Chow, 1959): **n = 0.04 s/(m^(1/3))**  
("manningseq" in supplementary material from Rosenwinkel et al. (2017), by Schwanghart)

**Input data for code `allochthonous_boulders_for_paleohydrology.m`**

Table S2-1: Boulders import table:

sample name	intermediate diameter [m]	density of boulder rock material [kg/m <sup>3</sup> ]	topoprofiles
NEQ/161 01	8.7	2800	11,12
NEQ/161 02	4.5	2800	11,12
NEQ/161 03	29.9	2800	11,12
NEQ/162 44	9.2	2800	6,7
NEQ/162 45	9.9	2800	6,7
NEQ/162 46	12.5	2800	6,7
NEQ/162 47	18	2700	6,7
NEQ/162 58	13.4	2700	1,2
NEQ/162 59	8.5	2800	1,2
NEQ/162 60	18.6	2700	3,4
NEQ/162 61	14.7	2700	3,4
NEQ/162 66	8.8	2700	3,4
NEQ/162 67	9.9	2700	3,4
NEQ/162 79	9.5	2800	9,10
NEQ/162 80	11.4	2800	9,10
NEQ/162 98	9.4	2800	9,10



Table S2-2.3: Topoprofile import table (3)

topo11			topo12			topo13											
27°43'44.73"N, 85°46'45.76"E			27°43'41.55"N, 85°46'44.38"E			27°43'28.60"N, 85°46'41.86"E											
d_11	z_11	S_11	d_12	z_12	S_12	d_13	z_13	S_13	d_14	z_14	S_14	d_15	z_15	S_15	d_16	z_16	S_16
0	1000	0.006	0	1000	0.006	0	1000	0.006	213.9	960							
48.5	960		69.5	960		534.8	920										
90.9	920		128.3	920		625.7	880										
171.1	880		197.9	880		673.8	840										
240.6	840		235.3	840		850.3	800										
294.1	800		320.9	800													
342.2	760		390.4	760		898.4	760										
395.7	720		443.9	720		935.8	720										
449.2	680		513.4	680		1048.1	680										
459.9	671		540.1	670		1069.5	667										
545.5	671		609.6	670		1144.4	667										
550.8	680		625.7	680		1155.1	680										
582.9	720		668.4	720		1326.2	720										
636.4	760		695.2	760		1417.1	760										
684.5	800		743.3	800		1470.6	800										
738	840		780.7	840		1679.1	840										
812.8	880		850.3	880		1802.1	880										
844.9	920		898.4	920		1844.9	920										
903.7	960		984	960		1909.1	960										
973.3	1000		1155.1	1000		1978.6	1000										

**Output data from code `allochthonous_boulders_for_paleohydrology.m`**

Table S2-3: Paleohydrology results from boulders

sample name	boulder diameter [m]	density of boulder rock material [kg/m^3]	topoprofile s used for calculation	Flow velocity [m/s]			Flow discharge [m3/s]			Flow height [m]		
				Costa (1983)	Clarke (1996)	Alexander& Cooker (2016)	Costa (1983)	Clarke (1996)	Alexander& Cooker (2016)	Costa (1983)	Clarke (1996)	Alexander& Cooker (2016)
NEQ/161 01	8.7	2800	11,12	10.2	9.3	6.0	1.64E+04	1.25E+04	3.39E+03	15.9	13.7	6.4
NEQ/161 02	4.5	2800	11,12	7.8	6.7	4.3	7.29E+03	4.62E+03	1.34E+03	10.0	7.7	3.7
NEQ/161 03	29.9	2800	11,12	16.7	17.3	11.2	8.95E+04	1.03E+05	2.25E+04	40.5	43.6	19.0
NEQ/162 44	9.2	2800	6,7	10.4	9.6	6.2	1.31E+05	1.02E+05	2.13E+04	27.2	24.5	12.6
NEQ/162 45	9.9	2800	6,7	10.7	10.0	6.4	1.44E+05	1.15E+05	2.44E+04	28.3	25.7	13.4
NEQ/162 46	12.5	2800	6,7	11.8	11.2	7.2	1.97E+05	1.69E+05	3.74E+04	32.2	30.2	16.1
NEQ/162 47	18	2700	6,7	13.6	12.9	8.3	3.27E+05	2.74E+05	6.19E+04	40.1	37.1	20.0
NEQ/162 58	13.4	2700	1,2	12.1	10.8	7.2	1.10E+04	8.16E+03	2.56E+03	6.4	5.4	2.8
NEQ/162 59	8.5	2800	1,2	10.1	9.0	6.0	6.74E+03	4.85E+03	1.53E+03	4.9	4.1	2.1
NEQ/162 60	18.6	2700	3,4	13.8	12.9	8.5	3.11E+04	2.47E+04	5.39E+03	16.0	14.3	6.6
NEQ/162 61	14.7	2700	3,4	12.5	11.5	7.5	2.19E+04	1.60E+04	3.63E+03	13.5	11.5	5.4
NEQ/162 66	8.8	2700	3,4	10.2	8.9	5.8	1.04E+04	6.43E+03	1.60E+03	9.3	7.2	3.4
NEQ/162 67	9.9	2700	3,4	10.7	9.4	6.2	1.23E+04	7.89E+03	1.92E+03	10.1	8.1	3.8
NEQ/162 79	9.5	2800	9,10	10.5	9.7	6.3	9.24E+03	6.98E+03	1.80E+03	12.1	10.4	4.8
NEQ/162 80	11.4	2800	9,10	11.3	10.6	6.9	1.19E+04	9.52E+03	2.37E+03	13.9	12.3	5.6
NEQ/162 98	9.4	2800	9,10	10.5	9.6	6.3	9.11E+03	6.86E+03	1.77E+03	12.0	10.3	4.7

### Supplement 3 (S3): Boulder exposure ages

Surface exposure dating with cosmogenic nuclides developed substantially in the last two decades and has become a powerful tool in analysing landscape evolution in Quaternary Geology and Geomorphology (e.g. Ivy-Ochs and Kober, 2008). Taking into account local cosmogenic nuclide production and topographic shielding, which lowers production, a surface exposure age is calculated from the cosmogenic nuclide concentrations by solving for  $t$  in Equation S3-1 below, where nuclide concentration  $N$  [atoms g<sup>-1</sup>] is given as a function of time  $t$  [a] with production rate  $P$  [atoms g<sup>-1</sup> a<sup>-1</sup>] and decay constant  $\lambda$  [a<sup>-1</sup>]. Equation S3-1 simplifies the evolution of cosmogenic nuclide concentrations by neglecting inheritance and erosion. Following standard chemical separation procedures (details provided below), concentrations of cosmogenic nuclides are measured with accelerated mass spectrometry (AMS). The radionuclide <sup>10</sup>Be (<sup>16</sup>O(n,4p3n)<sup>10</sup>Be) is used in this study for cosmogenic nuclide dating because the target mineral quartz (SiO<sub>2</sub>) is abundant in the sampled lithologies. Exposure dating with <sup>10</sup>Be is a well-established method, comparably easy to apply and delivers reliable results for the targeted time-frame (Dunai, 2010).

$$N(t) = \frac{P}{\lambda} \times (1 - e^{-\lambda t}) \quad (\text{S3-1})$$

#### Laboratory work

Sample preparation was performed in the laboratories of the Geological Institute in the Earth Science Department at ETH Zurich. The procedure employed is based on Ivy-Ochs (1996) with modifications from Norton et al. (2008), which itself is adapted after Von Blanckenburg et al. (1996, 2004). Samples were crushed with high-voltage pulse power fragmentation (SELFRAg), sieved to grain sizes between 1000 µm to 250 µm and magnetically separated to remove unwanted magnetic minerals from each sample. Repetitive acid treatment with diluted hydrochloric (HCl), hexafluorosilicic (H<sub>2</sub>SiF<sub>6</sub>) and hydrofluoric (HF) acids was used to remove minerals, mainly oxides, carbonates and feldspars from the sample material and isolate quartz (Norton et al. 2008). In order to fully remove meteoric <sup>10</sup>Be from the remaining crystals, the grain boundaries of the quartz were leached with HF 3 times so as to dissolve 10% of the quartz mass at each step. Approximately 200 to 250 µg <sup>9</sup>Be carrier solution was added to a sample weight of ~50 g to enable appropriate sample size and isotope ratio for a later measurement. Beryllium was then extracted and purified using ion exchange column chromatography. The final steps before measurement, including pressing and loading of the samples into cathodes, were performed at the Ion Beam Laboratory at ETH Zurich, Hönggerberg where the samples were measured at the LIP 0.5 MV compact accelerator mass spectrometry (AMS) facility (Tandy).

Results were normalized to secondary in-house standards S2007N and S2010N with nominal values of <sup>10</sup>Be/<sup>9</sup>Be = 28.1 × 10<sup>-12</sup> and <sup>10</sup>Be/<sup>9</sup>Be = 3.3 × 10<sup>-12</sup>, respectively. S2007N and S2010N have been calibrated with our new primary standard ICN 01-5-1. ICN 01-5-1 is produced by K. Nishiizumi and has a nominal <sup>10</sup>Be/<sup>9</sup>Be value of 2.709 × 10<sup>-11</sup> (Nishiizumi et al., 2007, Christl et al., 2013). Blank corrections were performed using an arithmetic mean of 14 <sup>10</sup>Be blanks with zero outliers measured at the Tandy facility in the period of 4 months before our last measurement was conducted (20 blanks with one outlier in a period of one year before measurement for sample NEQ/162 79). AMS measurements were performed in June and September 2017 (June 2018 for sample NEQ/162 79).

#### Calculation of ages

Subsequently cosmogenic exposure ages were computed from the <sup>10</sup>Be/<sup>9</sup>Be ratios including analytical errors measured at the AMS facility. The “Cosmic Ray Exposure program” (CREp) code, which is accessible online via the URL <http://crep.crgp.cnrs-nancy.fr> (Martin et al., 2017), was used to calculate exposure ages from nuclide concentrations. This web-based computational tool was chosen because it utilizes a robust production rate calibration database set up by the Informal Cosmogenic-nuclide Exposure-age Database (ICE-D) project (<http://calibration.ice-d.org>). The database is continuously updated and compiles and aligns production rate calibration data published for a variety of locations globally (Martin et al., 2017). Parameters input into CREp include the <sup>10</sup>Be concentration in the samples (calculated from the measured ratios) with 1 $\sigma$ -error, sample location coordinates and altitude, topographic shielding, an assumed uniform rock sample density of 2.7 g cm<sup>-3</sup> and the average sample thickness. We applied the Lifton-Sato-Dunai (LSD) theoretical scaling scheme (Lifton et al., 2014) for our age computation which uses analytical approximations to modelled cosmic ray particle fluxes giving specific atmospheric cross-sections for the <sup>10</sup>Be-nuclide and the other particles involved in the corresponding nuclear reactions (Martin et al., 2017). Another input scheme is the ERA-40 atmosphere

model (Uppala et al., 2005) based on a 45 year spanning database of atmospheric pressures for any locations on earth. It gives a pressure distribution approximation necessary because atmospheric pressure has an impact on the local production rate of cosmogenic nuclides. The geomagnetic record Lifton 2016 VDM (Pavón-Carrasco et al., 2014; Laj et al., 2004; Ziegler et al., 2011) was chosen to account for variations in the earth's magnetic field in the past. We chose a global mean production rate because no production rate calibration data was available for the whole Asian continent (see full list of references on <http://crep.crgc.cnrs-nancy.fr> or Martin et al., 2017). We computed our ages on the 7<sup>th</sup> of June 2018.

**Table S3-1: Boulder exposure ages – results**

Sample #	River	Lat [°]	Lon [°]	Alt. [m a.s.l.] <sup>(1)</sup>	Sample thickness [cm]	Shielding	<sup>10</sup> Be/ <sup>9</sup> Be ratio [10 <sup>-14</sup> ]	1σ analytical error of ratio [%]	Sample weight [g]	Amou nt of carrier (μg) <sup>(2)</sup>	<sup>10</sup> Be [at/g] <sup>(3)</sup>	1σ AMS final error [%] <sup>(3)</sup>	Exposure age ± 1σ [ka BP] <sup>(4)</sup>
<u>NEQ/161_01</u>	SUNKOSHI	27.729	85.779	674	2.0	0.86	3.70	8.8	21.381	201.6	1.67 x 10 <sup>4</sup>	13.9	4.98 ± 0.65
<u>NEQ/161_02</u>	SUNKOSHI	27.728	85.779	672	3.0	0.93	1.02	15.3	40.957	256.4	9.18 x 10 <sup>2</sup>	95.8	maximum 0.49 <sup>(5)</sup>
<u>NEQ/161_03</u>	SUNKOSHI	27.724	85.778	686	6.5	0.95	14.83	5.1	34.978	201.9	5.28 x 10 <sup>4</sup>	5.6	13.28 ± 0.96
<u>NEQ/162_44</u>	TRISHULI	27.856	85.070	441	3.0	0.99	2.26	10.5	22.521	256.6	1.10 x 10 <sup>4</sup>	19.1	3.48 ± 0.67
<u>NEQ/162_45</u>	TRISHULI	27.856	85.069	440	3.0	0.99	6.48	6.6	43.087	201.7	1.69 x 10 <sup>4</sup>	8.5	5.22 ± 0.46
<u>NEQ/162_46</u>	TRISHULI	27.856	85.069	445	3.0	0.99	4.69	7.8	33.040	202.4	1.49 x 10 <sup>4</sup>	11.1	4.64 ± 0.54
<u>NEQ/162_47</u>	TRISHULI	27.856	85.068	445	2.5	0.99	4.81	7.5	41.518	257.1	1.64 x 10 <sup>4</sup>	9.7	5.05 ± 0.49
<u>NEQ/162_58</u>	TRISHULI	28.009	85.184	679	4.5	0.96	6.96	6.8	58.751	197.7	1.32 x 10 <sup>4</sup>	8.5	3.63 ± 0.35
<u>NEQ/162_59</u>	TRISHULI	28.009	85.184	680	4.0	0.95	2.15	10.8	37.292	200.9	4.03 x 10 <sup>3</sup>	26.2	1.06 ± 0.29
<u>NEQ/162_60</u>	TRISHULI	27.970	85.183	618	2.0	0.97	8.08	5.5	60.322	202.8	1.57 x 10 <sup>4</sup>	6.8	4.35 ± 0.37
<u>NEQ/162_61</u>	TRISHULI	27.969	85.182	609	1.5	0.97	4.26	7.1	40.426	254.7	1.44 x 10 <sup>4</sup>	9.7	4.01 ± 0.43
<u>NEQ/162_66a</u>	TRISHULI	27.970	85.180	630	2.0	0.98	9.52	5.7	61.306	201.7	1.85 x 10 <sup>4</sup>	6.7	4.82 ± 0.49 <sup>(6)</sup>
<u>NEQ/162_66b</u>	TRISHULI	27.970	85.180	630	2.0	0.98	4.25	10.6	41.450	304.8	1.74 x 10 <sup>4</sup>	13.0	
<u>NEQ/162_67</u>	TRISHULI	27.971	85.180	632	2.5	0.98	10.50	5.3	61.830	203.3	2.06 x 10 <sup>4</sup>	6.1	5.46 ± 0.38
<u>NEQ/162_79</u>	SUNKOSHI, Balephi Khola	27.735	85.780	683	1.5	0.96	6.65	14.3	39.027	251.1	2.46 x 10 <sup>4</sup>	16.7	6.23 ± 0.92
<u>NEQ/162_80</u>	SUNKOSHI	27.734	85.783	695	1.5	0.95	11.93	5.1	41.942	255.9	4.49 x 10 <sup>4</sup>	5.6	10.96 ± 0.73
<u>NEQ/162_98</u>	SUNKOSHI, Balephi Khola	27.741	85.777	693	1.5	0.90	5.05	8.2	40.199	256.3	1.79 x 10 <sup>4</sup>	10.3	4.97 ± 0.51

(1) elevation of sampling point

(2) 6.616 x 10<sup>19</sup> atoms <sup>9</sup>Be per gram carrier

(3) after blank correction: 1.36 x 10<sup>5</sup> ± 2.44 x 10<sup>4</sup> <sup>10</sup>Be atoms n = 14 blank measurements over 4 months in same laboratory (except for NEQ/162 79 that was corrected for a blank contribution of 1.43 x 10<sup>5</sup> ± 2.77 x 10<sup>4</sup> <sup>10</sup>Be atoms, n = 20 blank measurements over 1 year in same laboratory)

(4) calculated with online version of CREp (Martin et al.2017) on 7.6.2018, see text for set parameters and production rate.

(5) not statistically different from blank, yields only a maximum concentration

(6) age was calculated using the mean <sup>10</sup>Be concentrations from duplicate measurements NEQ/162 66A and NEQ/162 66B

## Boulders at Betrawati, Trishuli valley

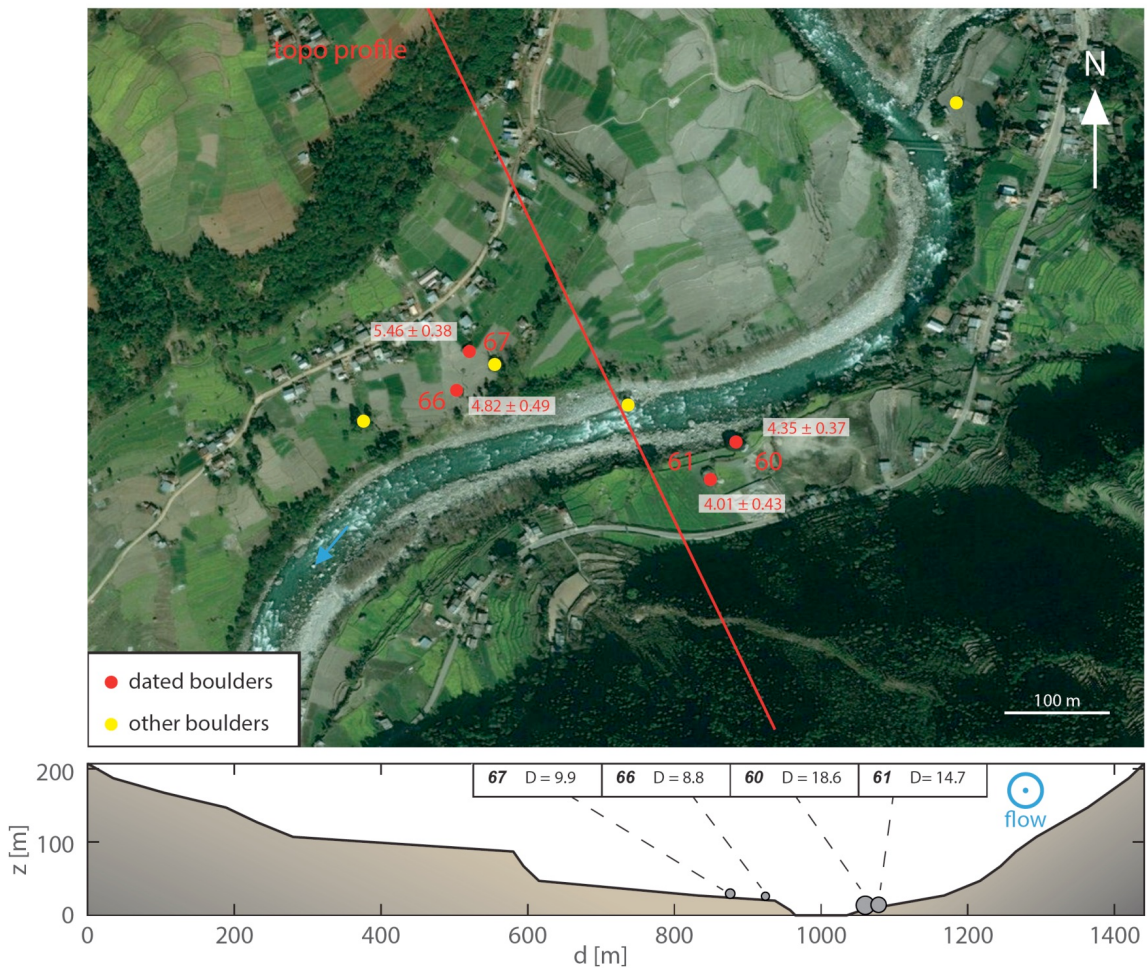


Figure S3-1: Top: Sample numbers are added without “NEQ/162...”. Exposure ages are in ka BP. Zoom-out on tributary fan. Red line shows location of topo-profile (bottom). Bottom: boulder intermediate diameters in meters. Bing Maps. (n.d.). [Satellite Imagery for central Nepal], Retrieved June to November 2017, from <https://www.bing.com/maps>, © Microsoft. Topographic profile drawn from topographic maps (see S2).

### Boulders south of Devighat, Trishuli valley



Figure S3-2: Top: Sample numbers are added without "NEQ/162...". Exposure ages are in ka BP. Middle: Zoom-out on tributary fan. Red line shows location of topo-profile (bottom). Bottom: boulder intermediate diameters in meters. Bing Maps. (n.d.). [Satellite Imagery for central Nepal], Retrieved June to November 2017, from <https://www.bing.com/maps>, © Microsoft. Topographic profile drawn from topographic maps (see S2).



## References

- Abramowski, U., 2004. The use of  $^{10}\text{Be}$  surface exposure dating of erratic boulders in the reconstruction of the late Pleistocene glaciation history of mountainous regions, with examples from Nepal and Central Asia.
- Christl, M., Vockenhuber, C., Kubik, P., Wacker, L., Lachner, J., Alfimov, V. and Synal, H.-A., 2013. The ETH Zurich AMS facilities: Performance parameters and reference materials. Nuclear Instruments and Methods in Physics Research Section B: Beam Interactions with Materials and Atoms, 294: 29-38.
- Dunai, T.J., 2010. Cosmogenic Nuclides: Principles, concepts and applications in the Earth surface sciences. Cambridge University Press.
- Finkel, R.C., Owen, L.A., Barnard, P.L. and Caffee, M.W., 2003. Beryllium-10 dating of Mount Everest moraines indicates a strong monsoon influence and glacial synchronicity throughout the Himalaya. *Geology*, 31(6): 561-564.
- Gayer, E., Lavé, J., Pik, R. and France-Lanord, C., 2006. Monsoonal forcing of Holocene glacier fluctuations in Ganesh Himal (Central Nepal) constrained by cosmogenic  $^3\text{He}$  exposure ages of garnets. *Earth and Planetary Science Letters*, 252(3-4): 275-288.
- Ivy-Ochs, S.D., 1996. The Dating of Rock Surfaces Using in Situ Produced  $^{10}\text{Be}$ ,  $^{26}\text{Al}$  and  $^{36}\text{Cl}$ : With Examples from Antarctica and the Swiss Alps. Diss. Naturwiss., Doctoral Thesis Thesis, ETH Zurich.
- Ivy-Ochs, S. and Kober, F., 2008. Surface exposure dating with cosmogenic nuclides. *Quaternary Science Journal*, 57(1-2): 179-209.
- Laj, C., Kissel, C. and Beer, J., 2004. High Resolution Global Paleointensity Stack Since 75 kyr (GLOPIS-75) Calibrated to Absolute Values. *Timescales of the Paleomagnetic Field*: 255-265.
- Martin, L., Blard, P.-H., Balco, G., Lavé, J., Delunel, R., Lifton, N. and Laurent, V., 2017. The CREp program and the ICE-D production rate calibration database: A fully parameterizable and updated online tool to compute cosmic-ray exposure ages. *Quaternary geochronology*, 38: 25-49.
- Nishiizumi, K., Imamura, M., Caffee, M.W., Southon, J.R., Finkel, R.C. and McAninch, J., 2007. Absolute calibration of  $^{10}\text{Be}$  AMS standards. Nuclear Instruments and Methods in Physics Research Section B: Beam Interactions with Materials and Atoms, 258(2): 403-413.
- Norton, K.P., von Blanckenburg, F., Schlunegger, F., Schwab, M. and Kubik, P.W., 2008. Cosmogenic nuclide-based investigation of spatial erosion and hillslope channel coupling in the transient foreland of the Swiss Alps. *Geomorphology*, 95(3): 474-486.
- Pavón-Carrasco, F.J., Osete, M.L., Torta, J.M. and De Santis, A., 2014. A geomagnetic field model for the Holocene based on archaeomagnetic and lava flow data. *Earth and Planetary Science Letters*, 388: 98-109.
- Pratt-Sitaula, B., Burbank, D.W., Heimsath, A. and Ojha, T., 2004. Landscape disequilibrium on 1000–10,000 year scales Marsyandi River, Nepal, central Himalaya. *Geomorphology*, 58(1): 223-241.
- Schaefer, J.M., Oberholzer, P., Zhao, Z., Ivy-Ochs, S., Wieler, R., Baur, H., Kubik, P.W. and Schlüchter, C., 2008. Cosmogenic beryllium-10 and neon-21 dating of late Pleistocene glaciations in Nyalam, monsoonal Himalayas. *Quaternary Science Reviews*, 27(3): 295-311.
- Uppala, S.M., Kållberg, P., Simmons, A., Andrae, U., Bechtold, V.d., Fiorino, M., Gibson, J., Haseler, J., Hernandez, A. and Kelly, G., 2005. The ERA-40 re-analysis. *Quarterly Journal of the royal meteorological society*, 131(612): 2961-3012.
- Von Blanckenburg, F., Belshaw, N. and O'Nions, R., 1996. Separation of  $^9\text{Be}$  and cosmogenic  $^{10}\text{Be}$  from environmental materials and SIMS isotope dilution analysis. *Chemical Geology*, 129(1-2): 93-99.
- Von Blanckenburg, F., Hewawasam, T. and Kubik, P.W., 2004. Cosmogenic nuclide evidence for low weathering and denudation in the wet, tropical highlands of Sri Lanka. *Journal of Geophysical Research: Earth Surface*, 109(F3).
- Ziegler, A.D., Wasson, R.J., Bhardwaj, A., Sundriyal, Y., Sati, S., Juyal, N., Nautiyal, V., Srivastava, P., Gillen, J. and Saklani, U., 2014. Pilgrims, progress, and the political economy of disaster preparedness—the example of the 2013 Uttarakhand flood and Kedarnath disaster. *Hydrological Processes*, 28(24): 5985-5990.